ACE2-like carboxypeptidase B38-CAP protects from SARS-CoV-2-induced lung injury

Tomokazu Yamaguchi
Department of Biochemistry and Metabolic Science, Akita University Graduate School of Medicine, 1-1-1 Hondo, Akita 010-8543, Japan

Midori Hoshizaki
Department of Biochemistry and Metabolic Science, Akita University Graduate School of Medicine, 1-1-1 Hondo, Akita 010-8543, Japan; Laboratory of Regulation of Intractable Infectious Diseases, National Institute of Biomedical Innovation, Health and Nutrition (NIBIOHN), 7-6-8 Saito-Asagi, Ibaraki, Osaka 567-0085, Japan

Takafumi Minato
Department of Biochemistry and Metabolic Science, Akita University Graduate School of Medicine, 1-1-1 Hondo, Akita 010-8543, Japan

Satoru Nirasawa
Biological Resources and Post-Harvest Division, Japan International Research Center for Agricultural Sciences, 1-1 Ohwashi, Tsukuba, Ibaraki 305-8686, Japan

Masamitsu N Asaka
Tsukuba Primate Research Center, NIBIOHN, Hachimandai 1-1, Tsukuba-shi, Ibaraki 305-0843, Japan

Mayumi Niiyama
Laboratory of Biopharmaceutical Research, NIBIOHN, 7-6-8 Saito-Asagi, Ibaraki, Osaka 567-0085, Japan

Masaki Imai
Division of Virology, Department of Microbiology and Immunology, Institute of Medical Science, University of Tokyo, 108-8639 Tokyo, Japan

Akihiko Uda
Department of Veterinary Science, National Institute of Infectious Diseases, 1-23-1 Toyama, Shinjyuku-ku, Tokyo, 162-8640, Japan

Jasper Fuk-Woo Chan
State Key Laboratory of Emerging Infectious Diseases, Carol Yu Centre for Infection, Department of Microbiology, Li Ka Shing Faculty of Medicine, The University of Hong Kong, Pokfulam, Hong Kong Special Administrative Region, China

Saori Takahashi
Akita Research Institute of Food and Brewing, 4-26 Sanuki, Arayamachi, Akita 010-1623, Japan

Jianbo An
Department of Biochemistry and Metabolic Science, Akita University Graduate School of Medicine, 1-1-1 Hondo, Akita 010-8543, Japan

Akari Saku
Department of Biochemistry and Metabolic Science, Akita University Graduate School of Medicine, 1-1-1 Hondo, Akita 010-8543, Japan
Ryota Nukiwa
Laboratory of Regulation of Intractable Infectious Diseases, National Institute of Biomedical Innovation, Health and Nutrition (NIBIOHN), 7-6-8 Saito-Asagi, Ibaraki, Osaka 567-0085, Japan; Department of Anesthesiology and Intensive Care Medicine, Osaka University Graduate School of Medicine, Osaka 565-0871, Japan
Daichi Utsumi
Tsukuba Primate Research Center, NIBIOHN, Hachimandai 1-1, Tsukuba-shi, Ibaraki 305-0843, Japan
Maki Kiso
Division of Virology, Department of Microbiology and Immunology, Institute of Medical Science, University of Tokyo, 108-8639 Tokyo, Japan
Atsuhiro Yasuhara
Division of Virology, Department of Microbiology and Immunology, Institute of Medical Science, University of Tokyo, 108-8639 Tokyo, Japan
Vincent Kwok-Man Poon
State Key Laboratory of Emerging Infectious Diseases, Carol Yu Centre for Infection, Department of Microbiology, Li Ka Shing Faculty of Medicine, The University of Hong Kong, Pokfulam, Hong Kong Special Administrative Region, China
Chris Chung-Sing Chan
State Key Laboratory of Emerging Infectious Diseases, Carol Yu Centre for Infection, Department of Microbiology, Li Ka Shing Faculty of Medicine, The University of Hong Kong, Pokfulam, Hong Kong Special Administrative Region, China
Yuji Fujino
Department of Anesthesiology and Intensive Care Medicine, Osaka University Graduate School of Medicine, Osaka 565-0871, Japan
Satoru Motoyama
Department of Surgery, Akita University Graduate School of Medicine, 1-1-1 Hondo, Akita 010-8543, Japan
Satoshi Nagata
Laboratory of Antibody Design, NIBIOHN, 7-6-8 Saito-Asagi, Ibaraki, Osaka 567-0085, Japan
Josef M. Penninger
Department of Medical Genetics, Life Sciences Institute, University of British Columbia, 2350 Health Sciences Mall, Vancouver, BC Canada, V6T 1Z3; IMBA, Institute of Molecular Biotechnology of the Austrian Academy of Sciences; 1030, Vienna; Austria
Haruhiko Kamada
5Laboratory of Biopharmaceutical Research, NIBIOHN, 7-6-8 Saito-Asagi, Ibaraki, Osaka 567-0085, Japan
Kwok-Yung Yuen

State Key Laboratory of Emerging Infectious Diseases, Carol Yu Centre for Infection, Department of Microbiology, Li Ka Shing Faculty of Medicine, The University of Hong Kong, Pokfulam, Hong Kong Special Administrative Region, China

Wataru Kamitani

Department of Infectious Diseases and Host Defense, Graduate School of Medicine, Gunma University, Maebashi, Gunma 371-8511, Japan

Ken Maeda

Department of Veterinary Science, National Institute of Infectious Diseases, 1-23-1 Toyama, Shinjyuku-ku, Tokyo, 162-8640, Japan

Yoshihiro Kawaoka

Division of Virology, Department of Microbiology and Immunology, Institute of Medical Science, University of Tokyo, 108-8639 Tokyo, Japan

Yasuhiro Yasutomi

Tsukuba Primate Research Center, NIBIOHN, Hachimandai 1-1, Tsukuba-shi, Ibaraki 305-0843, Japan

Yumiko Imai

Laboratory of Regulation of Intractable Infectious Diseases, National Institute of Biomedical Innovation, Health and Nutrition (NIBIOHN), 7-6-8 Saito-Asagi, Ibaraki, Osaka 567-0085, Japan

Keiji Kuba (kuba@med.akita-u.ac.jp)

Department of Biochemistry and Metabolic Science, Akita University Graduate School of Medicine, 1-1-1 Hondo, Akita 010-8543, Japan https://orcid.org/0000-0002-2203-5293

Research Article

Keywords: SARS-CoV-2, Angiotensin-converting enzyme 2, ACE2, angiotensin, COVID-19, lung injury, ARDS, B38-CAP, cytokine, Spike

Posted Date: July 16th, 2021

DOI: https://doi.org/10.21203/rs.3.rs-124634/v2

Version of Record: A version of this preprint was published at Nature Communications on November 23rd, 2021. See the published version at https://doi.org/10.1038/s41467-021-27097-8.

Abstract

Angiotensin-converting enzyme 2 (ACE2) is a receptor for cell entry of SARS-CoV-2, and recombinant soluble ACE2 protein inhibits SARS-CoV-2 infection as a decoy. ACE2 is a carboxypeptidase that degrades angiotensin II (Ang II) to angiotensin 1-7 (Ang 1-7) and thereby improves the pathologies of cardiovascular disease or acute lung injury. To address whether the carboxypeptidase activity of ACE2 is protective in COVID-19, we investigated the effects of B38-CAP, an ACE2-like enzyme, on SARS-CoV-2-induced lung injury. Expression of endogenous ACE2 protein was significantly downregulated in the lungs of SARS-CoV-2-infected hamsters or SARS-CoV-2 challenged human ACE2 transgenic mice, leading to elevation of Ang II levels. *In vivo* administration of recombinant SARS-CoV-2 Spike also downregulated ACE2 expression, elevated Ang II levels and considerably worsened the symptoms of acute lung injury in hamsters exposed to acid aspiration. Despite its ACE2-like catalytic core, B38-CAP neither bound to Spike nor neutralized cell entry of SARS-CoV-2. However, treatment with B38-CAP improved the pathologies of Spike-augmented acid-induced lung injury. In SARS-CoV-2-infected hamsters, B38-CAP significantly improved lung edema and pathologies of lung injury and downregulated IL-6 levels without affecting viral RNA loads. Moreover, in human ACE2 transgenic mice, B38-CAP also attenuated SARS-CoV-2-induced lung edema and pathologies and improved lung functions. These results provide the first experimental *in vivo* evidence that increasing ACE2-like enzymatic activity is a potential therapeutic strategy to alleviate lung pathologies in COVID-19.

Introduction

Severe acute respiratory syndrome coronavirus (SARS coronavirus or SARS-CoV) emerged in 2003 as an epidemic of highly contagious and deadly respiratory disease [1-3]. In December 2019, a new coronavirus, SARS-CoV-2 was first identified in a pneumonia outbreak in Wuhan, China, and spread rapidly all over the world in a few months, leading to the current pandemic[4,5]. Infection of this virus causes Coronavirus Disease 2019 (COVID-19) with respiratory symptoms ranging from mild disease to severe acute lung injury/acute respiratory distress syndrome (ARDS) and multi-organ failure with high mortality, especially in patients with cardiovascular diseases, diabetes or advanced age [6-8]. Angiotensin-converting enzyme 2 (ACE2) was identified as a receptor for entry of SARS coronavirus into host cells *in vitro* and *in vivo* [9,10]. The Spike (S) protein in SARS-CoV-2 shares structural similarities with the Spike in SARS coronavirus, and SARS-CoV-2 is also shown to utilize ACE2 as a receptor for cell entry *in vitro* [4,11,12].

ACE2 was originally described as the enzyme homologous to angiotensin-converting enzyme (ACE) in 2000 [13,14]. The renin–angiotensin system (RAS) maintains blood pressure and fluid balance [15,16], while ACE2 has been shown to be an important protective factor in several disease states including heart failure, myocardial infarction, hypertension, acute lung injury or diabetes [17]. When the RAS is activated, ACE as a carboxypeptidase cleaves angiotensin I to generate the vasopressor octapeptide angiotensin II (Ang II). ACE2 is a negative regulator of the RAS, which catalyzes degradation of Ang II to Ang 1-7, thereby counterbalancing ACE activity [13,14]. RAS activation has been shown to worsen the pathologies of

ARDS/acute lung injury [18]. ACE2 expression is downregulated in the lungs of mice under acute lung injury induced by various causes including acid aspiration, sepsis and lethal influenza infection [18-20]. Loss of ACE2 augments acute lung injury through Ang II upregulation, whereas treatment with recombinant soluble ACE2, which is devoid of membrane-anchored domain, improves lung injury in animal models [18]. ACE2 expression was also markedly downregulated in the lungs of SARS coronavirus-infected mice, and injecting Spike protein of the SARS coronavirus into mice down-modulates ACE2 expression, thereby worsening lung injury through RAS activation [10,18]. Although early studies on SARS-CoV-2 suggested that mRNA expression of ACE2 was upregulated in certain subsets of cells in SARS-CoV-2 infected lungs [21], this upregulation appears to generate a truncated ACE2 isoform that cannot bind to Spike and lacks catalytic activity [22].

Treatment with recombinant soluble human ACE2 protein (rshACE2) was demonstrated to exert beneficial effects in various disease models including heart failure and diabetic nephropathy as well as acute lung injury [18,23,24]. rshACE2 has been developed as a therapeutic for treating patients with ARDS/acute lung injury. In addition, rshACE2 was recently shown to bind to SARS-CoV-2 Spike, thereby suppressing the infection of SARS-CoV-2 in cell lines and human stem-engineered organoids *in vitro* [25]. Thus, rshACE2 functions both as a decoy to inhibit cell entry of SARS-CoV-2 and as an enzyme to protect from lung injury. However, the significance of ACE2 enzymatic activity in COVID-19 remains elusive. We have recently identified bacteria-derived carboxypeptidase B38-CAP as an ACE2-like enzyme [26]. Recombinant B38-CAP protein catalyzes the conversion of Ang II to Ang 1-7 as well as hydrolysis of other ACE2 substrate peptides including des-Arg^9-bradykinin, apelin and dynorphin A, with the same potency as ACE2 [26,27]. Treatment with B38-CAP downregulates Ang II levels in mice and thereby antagonizes Ang II-induced hypertension and improves heart failure without overt toxicities [26].

In this study, we aimed to investigate the impacts of ACE2 enzymatic activity on acute lung injury induced by SARS-CoV-2 infection. We show that SARS-CoV-2-infection or Spike protein downregulates ACE2 expression. B38-CAP as an ACE2-like enzyme, but not as a decoy for the virus, improves the symptoms of SARS-CoV-2-induced lung injury as well as virus-free Spike-augmented lung injury. These results have important therapeutic implications to use rshACE2 or RAS inhibitors for COVID-19 patients, for which beneficial outcomes have recently been suggested in clinical studies [28,29].

Results

Downregulation of ACE2 protein expression by SARS-CoV-2 infection and Spike protein.

To determine the effects of SARS-CoV-2 infection on ACE2 protein expression in the lungs (Fig. 1a), we infected hamsters with SARS-CoV-2 (UT-NCGM02) through intranasal inoculation [30,31]. At 4 days after infection, while viral Nucleocapsid phosphoprotein (NP) was highly expressed in the lungs, expression of ACE2 protein or mRNA was significantly downregulated in the lungs of SARS-CoV-2-infected hamsters (Fig. 1b, c; Extended Data Fig. 1a), and consistent results were obtained with a different isolate of the

virus (HKU-001a) (Extended Data Fig. 1b). We reasoned that reduced ACE2 expression might affect the lung pathologies of SARS-CoV-2 infection as seen in the mice infected with SARS coronavirus [10]. To test this, we prepared three constructs for recombinant proteins of SARS-CoV-2 Spike; trimeric Spike (1-1208 amino acids) with 6 proline substitutions retaining the prefusion conformation [32], S1 domain (1-685 amino acids) and receptor-binding domain (RBD) (319-541 amino acids) fused to human Fc, described hereafter as Spike-6P, S1-Fc and RBD-Fc, respectively (Fig. 1d). We expressed and purified Spike-6P, S1-Fc and RBD-Fc proteins in 293 cells (Extended Data Fig. 1c). In *in vitro* pull-down assays, all the recombinant Spike proteins indeed bound to human ACE2 and hamster Ace2 (Fig. 1e; Extended Data Fig. 1d-g). Since recombinant Spike or RBD of the SARS coronavirus downregulates ACE2 expression [10,33], we examined the effects of SARS-CoV-2 Spike protein on ACE2 expression. We treated Vero E6 cells with RBD-Fc and analyzed expression of endogenous ACE2 on the cell surface. RBD-Fc bound to endogenous ACE2 in Vero E6 cells (Fig. 1f, g). Decreased binding of RBD-Fc to ACE2 at 37^{o}C compared with at 4^{o}C suggested that expression of ACE2 protein on the cell surface was downregulated by RBD-Fc, partly through internalization or shedding as previously described for SARS coronavirus [33,34] (Fig. 1f, g).

We determined whether SARS-CoV-2 Spike proteins downregulate Ace2 expression *in vivo* (Fig. 1h). When hamsters were treated with S1-Fc, RBD-Fc or control-Fc (11 nmol/kg for each), immunohistochemistry with anti-human Fc antibody showed that S1-Fc and RBD-Fc but not control-Fc localized in the lungs of hamsters (Fig. 1i). In the absence of acid-induced injury, treatment with S1-Fc (11 nmol/kg), RBD-Fc (11 nmol/kg) or Spike-6P (3.7 nmol/kg) did not strikingly affect the abundance of Ace2 protein in the lungs compared with control-Fc or vehicle treatment, though RBD-Fc showed a slight but statistically significant decrease (Fig. 1j, k; Extended Data Fig. 1h, i). On the other hand, when acute lung injury was introduced to hamsters with intra-tracheal instillation of acid (0.1 M HCl, 100 ml) and kept without mechanical ventilation support (Fig. 1f), treatment with S1-Fc, RBD-Fc or Spike-6P significantly downregulated the abundance of Ace2 protein in the lungs (Fig.1j-m). Consistently, plasma Ang II levels were significantly upregulated by Spike-6P, S1-Fc or RBD-Fc in the hamsters with acute lung injury but not in the absence of lung injury (Fig. 2c; Extended Data Fig. 2a). Thus, SARS-CoV-2 Spike downregulates ACE2 protein expression *in vitro*, and Spike treatment plus acid-induced injury downregulates pulmonary ACE2 expression levels and induces RAS activation *in vivo*.

SARS-CoV-2 Spike protein worsens acute lung injury

Without acid instillation the Spike proteins-injected hamsters were apparently healthy. S1-Fc (11 nmol/kg)-treated hamsters induced mild lung edema as defined by wet weight to dry weight ratio of the lungs (Wet/Dry ratio) (Extended Data Fig. 2b, c), whereas treatment with RBD-Fc (11 nmol/kg) or Spike-6P (3.7 nmol/kg) showed non-significant increase of Wet/Dry ratio (Fig. 2d, e; Extended Data Fig. 2b, c). Histological analysis also showed non-significant mild pathologies in Spike-6P-treated lungs (Fig. 2f, g), though S1-Fc or RBD-Fc exhibited significant increase of lung injury scores (Extended Data Fig. 2d, e). Although the effects of S1-Fc or RBD-Fc may contain activation of immune cells by Fc moiety in the fusion construct (Fig. 1d), Spike protein *per se* is potentially pro-inflammatory in the lungs.

We next examined the effects of Spike proteins on acid-induced lung injury (Fig. 1h). At 24 hours after acid aspiration the lungs appeared mildly reddish and swollen with occasional hemorrhagic spots in control-Fc or vehicle-treated hamsters (Fig. 2d; Extended Data Fig. 2b). When Spike-6P, S1-Fc or RBD-Fc was intraperitoneally injected in addition to acid instillation, the hamsters exhibited severe lung injury with massive inflammation and hemorrhage (Fig. 2d; Extended Data Fig. 2b) and showed significant increase of wet to dry weight ratio of the lungs (Fig. 2e; Extended Data Fig. 2c), indicating that Spike protein augmented lung edema. Consistently, histological analysis showed the pathologies of severe lung inflammation in Spike (Spike-6P, S1-Fc or RBD-Fc) plus acid-treated hamsters (Fig. 2f, g; Extended Data Fig. 2d, e). Thus, SARS-CoV-2 Spike protein exacerbates acid-induced lung injury.

B38-CAP suppresses SARS-CoV-2 Spike-induced lung injury.

Recombinant human soluble ACE2 degrades Ang II while binds to RBD of the Spike thereby inhibiting the entry of SARS-CoV-2 into cells (Fig. 2a). We first examined whether B38-CAP binds to RBD-Fc protein *in vitro*. While soluble ACE2 was efficiently co-immunoprecipitated with RBD-Fc, B38-CAP was not pulled down with RBD-Fc (Extended Data Fig. 3a, b). In addition, when B38-CAP was added to the *in vitro* culture of SARS-CoV-2-infected Vero E6/TMPRSS2 cells, viral replication was not affected by B38-CAP (Extended Data Fig. 3c, d). Thus, B38-CAP is an ACE2-like enzyme lacking the ability to inhibit cell entry of SARS-CoV-2. We intraperitoneally injected B38-CAP (2 mg/kg per injection) to the hamsters under acid-induced lung injury with Spike treatment (Spike-6P or RBD-Fc) (Fig. 2b). At 2 hours after last injection of B38-CAP or vehicle, ACE2-like enzymatic activity was markedly elevated in the plasma of B38-CAP-treated hamsters (Extended Data Fig. 4a). Measured ACE2 activity may contain the activity of endogenous soluble ACE2 in addition to injected B38-CAP. However, soluble ACE2 is not expressed by alternative splicing in transcription but generated by post-translational mechanisms [35], and B38-CAP does not induce shedding of ACE2 from the cell surface. Thus, we interpreted that the measured ACE2 activity primarily represents injected B38-CAP in circulation. In line with increased ACE2 activity, elevated Ang II levels were significantly downregulated in the plasma of B38-CAP-treated hamsters compared with vehicle-treated ones (Fig. 2c; Extended Data Fig. 4b), and Ang 1-7 levels tended to show a slight upregulation (Extended Data Fig. 4c), indicating that injected B38-CAP is functional as an ACE2-like enzyme to degrade Ang II in hamsters. In the hamsters treated with acid only, B38-CAP significantly suppressed acid-induced formation of lung edema and downregulated wet to dry weight ratio of the lungs (Fig. 2d, e; Extended Data Fig. 4d, e). Importantly, in the hamsters under Spike plus acid-induced lung injury, severe inflammation and pulmonary edema was markedly attenuated by B38-CAP treatment (Fig. 2d, e; Extended Data Fig. 4d, e). Consistently, lung pathologies were significantly improved by B38-CAP (Fig. 2f, g; Extended Data Fig. 4f, g; Extended Data Table 2, 3). In addition, lung functions were measured as lung elastance and airway resistance. RBD-Fc plus acid-induced impairment of lung functions as evidenced by increased elastance and resistance were significantly improved by B38-CAP treatment (Fig. 2h, i). Furthermore, we examined mRNA expression of cytokines (IL-6, TNF-a and CXCL10) which are known to be upregulated in COVID-19 patients. While mRNA expression of IL-6, TNF-a and CXCL10 were also upregulated in Spike plus acid-treated hamsters, B38-CAP treatment significantly

downregulated high cytokine mRNA levels (Fig. 2j-l; Extended Data Fig. 4h-j). It should be noted that treatment with B38-CAP did not show any toxicities at least in kidney and liver function markers (Extended Data Fig. 4k-n). Therefore, B38-CAP suppresses Spike-induced severe lung injury.

B38-CAP mitigates lung injury induced by SARS-CoV-2 infection in hamsters.

To address the effects of B38-CAP in acute lung injury induced by SARS-CoV-2 infection, we treated SARS-CoV-2-infected hamsters with B38-CAP. We intratracheally inoculated hamsters with infectious SARS-CoV-2 stock virus at a dosage of 1 x 10^3 $TCID_{50}$ per animal. At 4 days post infection (dpi), high copy number of viral RNA (N gene) was detected in the lungs, and lung edema and pathologies and elevation of cytokine mRNAs were observed (Extended Data Fig. 5a-f). The lung pathologies and cytokine increase were more prominent in the hamsters with intratracheal infection than intranasal infection (not shown). At 12 hours after SARS-CoV-2 infection, we initiated the intraperitoneal injection of B38-CAP (2 mg/kg/day) to the hamsters (Fig. 3a). At 4 dpi, body weight decreased to less than 90% in both treatment groups with non-significant further decrease in B38-CAP-treated animals (Fig. 3b), whereas B38-CAP-treated hamsters were more active and appeared healthier than vehicle-treated ones (not shown). The hamsters were euthanized and lung tissues were harvested. When virus N RNA levels were measured as a readout for viral replication in the lungs, copy numbers of N RNA were comparable between B38-CAP treated hamsters and vehicle-treated ones (Fig. 3c), indicating that B38-CAP did not inhibit cell entry of the virus *in vivo*, similarly to *in vitro* results (Extended Data Fig. 3c, d). We next quantified Ang II levels in the lung tissues with ELISA. Ang II levels were significantly upregulated upon SARS-CoV-2 infection (Fig. 3d), consistent with downregulation of Ace2 expression (Fig. 1b; Extended Data Fig. 1a), whereas B38-CAP-treated hamsters showed a trend for reduction of Ang II levels in the lungs (Fig. 3d), suggesting that B38-CAP is functional as an ACE2-like carboxypeptidase in the infected hamsters. While SARS-CoV-2 infection induced lung edema as shown by increased lung weight to body weight ratio (LW/BW) (Fig. 3e) and elevated wet to dry ratio of lung weight (Fig. 3f), B38-CAP significantly improved lung edema as shown by decreased LW/BW and wet to dry ratio (Fig. 3e, f). In addition, histological analysis consistently showed that B38-CAP improved the lung pathologies (Fig. 3g), and lung injury score was significantly decreased in B38-CAP-treated hamsters compared with vehicle-treated hamsters (Fig. 3h); the scores of thick alveolar wall and hemorrhage were markedly decreased by B38-CAP treatment (Extended Data Table 4). Furthermore, IL-6 mRNA expression was significantly downregulated by B38-CAP treatment (Fig. 3i), and TNF-a mRNA expression also showed a trend for decrease (Fig. 3j), whereas CXCL-10 expression was not affected (Fig. 3k). Thus, B38-CAP has the ability to suppress inflammation and pathologies in the lungs of hamsters with SARS-CoV-2 infection.

Effects of B38-CAP on SARS-CoV-2-induced lung injury in human ACE2 transgenic mice.

We further investigated the effects of B38-CAP on SARS-CoV-2-induced lung injury by utilizing human ACE2 transgenic (hACE2 Tg) mice, in which expression of human ACE2 is ubiquitously induced by CAG promoter (Extended Data Fig. 6a, b). Human ACE2 protein was detected in the lungs of hACE2 Tg mice but not wild type mice (Fig. 4a). We intratracheally inoculated hACE2 Tg mice or wild type mice with

SARS-CoV-2 stock virus (UT-NCGM02) at a dosage of 2 x 10^3 $TCID_{50}$ per mouse. All the infected hACE2 Tg mice decreased body weight and were dead by 9 days after infection, whereas the virus-inoculated wild type mice appeared healthy during observation period (Extended Data Fig. 6c, d). Consistently, high copy number of viral N RNA were detected in the lungs of SARS-CoV-2 infected hACE2 Tg mice (Extended Data Fig. 6e). By contrast, wild type littermate mice were not apparently infected with the virus, though low amount of viral RNA was detected in one out of three mice at 2 dpi (Extended Data Fig. 6e), consistent with other recent studies showing no pathologies in wild type mice in the C57BL/6 background [36,37]. In SARS-CoV-2-infected hACE2 Tg mice, viral RNA (N) was highly detectable in brain, liver, spleen, kidney and colon as well as in the respiratory system (nasal turbinate, trachea and lung) (Extended Data Fig. 6f). The kinetics of viral infection varied among the organs. Virus titers and N RNA copy numbers in the lungs were peaked at 2 dpi and decreased through day 7 (Fig. 4b; Extended Data Fig. 6e), whereas the virus in brain became detectable at 4 dpi and markedly increased at day 7, in which viral load was the highest among the organs examined (Fig. 4c; Extended Data Fig. 6f), suggesting that SARS-CoV-2 replicates efficiently in brain. As for lung edema, wet to dry ratio of lung weight was significantly increased in SARS-CoV-2 infected lungs of hACE2 Tg mice, peaked at day 2 and day 4 post infection and normalized at day 7, whereas it was not changed after virus inoculation in wild type mice (Fig. 4d). In histopathological analysis, lung injury score was peaked at 4 days after infection and improved at day 7 in hACE2 Tg mice but not in wild type mice (Extended Data Fig. 7a, b). Consistently, pulmonary cytokine mRNA levels were peaked at day 2 with a sharp decline through day 7, and cytokines levels in the brain markedly elevated at 7 dpi in hACE2 Tg mice but not in wild type mice (Extended Data Fig. 7c, d). Interestingly, protein expression of both human ACE2 and mouse Ace2 was downregulated in the infected hACE2 Tg mice (Fig. 4e-g). Thus, SARS-CoV-2 infection in this hACE2 Tg mice induces severe lung injury through at 4 dpi, while the mice likely die of explosive viral replication and inflammation in the brain, which is consistent with high lethality of the mice expressing hACE2 in lung with brain inoculation of SARS-CoV-2 as recently shown [38].

We thus decided to evaluate the effects of B38-CAP on lung injury at 4 days after infection (Fig. 4h). At 4 dpi, decrease of body weight was comparable between B38-CAP-treated mice and vehicle-treated mice (Fig. 4i), and there was no difference in viral N RNA levels in the lungs between both treatment groups (Fig. 4j). In accordance with ACE2 downregulation, Ang II levels in the lung tissues were upregulated by SARS-CoV-2 infection (Fig. 4k). By contrast, supplementation of ACE2 activity by B38-CAP injection downregulated Ang II levels (Fig. 4k), whereas Ang 1-7 peptides were not detectable (not shown). B38-CAP significantly attenuated lung edema (Fig. 4l) and the lung pathologies (Fig. 4m), and lung injury score was decreased in B38-CAP-treated mice compared with vehicle-treated mice (Fig. 4n); the scores of alveolar congestion and wall thickness were significantly decreased in B38-CAP-treated animals (Extended Data Table 5). Increased cytokine expression in the lungs were not significantly improved by B38-CAP treatment, albeit IL-6 mRNA levels showed a trend for decrease in B38-CAP-treated mice (not shown). On the other hand, when lung function was measured for the infected hACE2 Tg mice, lung elastance and resistance were significantly decreased in B38-CAP-teated mice compared with vehicle-

treated mice (Fig. 4o, p). Thus, B38-CAP improves lung edema and impaired lung functions in hACE2 Tg mice with SARS-CoV-2-induced lung injury.

Discussion

In this study, we showed that SARS-CoV-2 infection or Spike injection plus acid aspiration decreased the protein abundance of ACE2 in the lungs of hamsters or hACE2 Tg mice, and that Spike downregulated expression of ACE2 protein in the cell culture by itself. B38-CAP was revealed to be an ACE2-like enzyme lacking the structure of a molecular decoy for the virus. We demonstrated that B38-CAP suppressed Spike plus acid-induced lung injury through downregulation of Ang II levels. We further demonstrated that B38-CAP improved pathologies of lung injury and impaired lung functions induced by SARS-CoV-2 infection in hamsters and hACE2 Tg mice without affecting viral replication.

SARS-CoV-2 infection decreases both protein and mRNA abundance of ACE2 in the lungs of hamsters. Although early studies of single-cell RNA-sequencing had suggested that interferon signaling upregulates ACE2 mRNA expression thereby potentially augmenting SARS-CoV-2 infection [21], it has been recently shown that interferon and virus induce expression of truncated ACE2 isoform, which is not functional as SARS-CoV-2 binding and carboxypeptidase [22]. Previous studies on 2003 SARS coronavirus had shown internalization or shedding of cell-surface ACE2 upon viral entry [33,34] as the mechanisms for ACE2 downregulation in the lungs of SARS coronavirus-infected animals [10]. Recently, in revision of this paper, Spike of the SARS-CoV-2 has been reported to downregulate ACE2 through ubiquitination [39]. On the other hand, downregulation of ACE2 expression had been not only seen in SARS or SARS-CoV-2 infection but also observed in other acute lung injuries caused by acid aspiration, LPS challenge or viral infection [18,20,40]. In our virus-free analyses, cell-surface expression of ACE2 was downregulated by Spike protein *in vitro*, and both protein and mRNA expression of ACE2 *in vivo* was downregulated by Spike treatment plus acid-induced injury. Despite a limitation in these analyses due to the absence of virus, the results suggested that there are two modes of ACE2 downregulation in SARS-CoV-2 infection; SARS-CoV-2 binding-mediated ACE2 internalization/shedding [33,34] and lung injury/inflammation-mediated downregulation [18,20,40]. Indeed, Although SARS-CoV-2 does not bind to mouse Ace2, downregulation of mouse Ace2 as well as human ACE2 was observed in hACE2 Tg mice (Fig. 4e-g). Intriguingly, mRNA expression of mouse Ace2 was also downregulated (not shown), suggesting that transcriptional/post-transcriptional mechanism may be involved in the ACE2 downregulation in COVID-19, such as NF-kB-induced microRNA-mediated downregulation of ACE2 mRNA [41]. In relation to the current mRNA vaccine strategies, it should be noted that the amount of mRNA vaccine-generated Spike protein in the body appears to be lower than in our experiments (injection of 1.3 mg/kg of Spike-6P protein in hamster).

Soluble ACE2 has a two-pronged approach for treating COVID-19; a carboxypeptidase to suppress lung injury and a decoy to neutralize SARS-CoV-2 infection. Since B38-CAP neither binds to RBD of the Spike nor inhibit viral replication *in vitro* and *in vivo*, the ACE2-like enzymatic activity of B38-CAP is crucial for its beneficial effects on lung injury of COVID-19. Interestingly, beneficial effects of B38-CAP in our COVID-

19 lung injury models were observed in the disease measures of lung edema, histopatholgies and respiratory function but not too much extent in cytokine expression. Improvement of lung edema and lung resistance may implicate that B38-CAP provides reduction of vascular permeability, water retention and/or microvascular tones to the microenvironment of SARS-CoV-2-induced lung injury. Accordingly, it would be speculated that therapeutics to suppress the RAS, such as angiotensin-receptor blocker (ARB) and ACE inhibitor, might be also beneficial for COVID-19 patients. In fact, although initial epidemiological studies showed that medication of ARB or ACE inhibitor did not affect infectivity of SARS-CoV-2 and severity of COVID-19 in the patients [42-44], recent clinical studies have suggested that ARB or ACE inhibitor provide better prognosis to the patients [28,29]. The enzymatic activity of both B38-CAP and ACE2 does not only degrade Ang II but also generates Ang 1-7, which is protective against lung injury through activation of the Mas receptor [45]. However, detection of low levels of Ang 1-7 suggests that Ang II degradation seems more important for B38-CAP's lung-protective effects than activation of Mas receptor. On the other hand, both ACE2 and B38-CAP target other peptide for its substrates. For instance, des-Arg^9-bradykinin is an agonist of B1 bradykinin receptor, and activation of the B1 receptor promotes lung injury [46,47], while ACE2 and B38-CAP degrade des-Arg^9-bradykinin [26,27]. Therefore, the beneficial effect of ACE2 enzymatic activity in SARS-CoV-2-induced lung injury might include the effects of degradation of other substrate peptides in addition to Ang II.

Although soluble ACE2 functional as both lung-protecting enzyme and decoy for the virus would be ideal for COVID-19 treatment, the efficacy of its decoy function in *in vivo* infection remains elusive. Focusing on enhanced conversion of Ang II without Spike binding, such as B38-CAP or soluble ACE2 mutated not to bind Spike, might be an alternate option to treat ARDS in COVID-19. In addition, development of B38-CAP as an inhalation drug might be advantageous, considering its cost-effective production and bacterial origin. Most of the drugs currently available for COVID-19 are re-positioned from other diseases or not specifically targeted for COVID-19. Our data show that ACE2 enzymatic activity is a potential therapeutic strategy to alleviate the symptoms of acute lung pathologies in COVID-19, further warranting the significance of specific molecular targeting in treating COVID-19.

Methods

Viruses

SARS-CoV-2 strain (UT-NCGM02) was maintained as previously described [31] , and virus from passages P3 was used in the experimental infection of hamsters at University of Tokyo. SARS-CoV-2 (Hong Kong strain, HKU-001a (GenBank: MT230904.1)) was maintained as previously described [30] and virus from passages P3 was used in the infection experiment of hamsters at the University of Hong Kong. For experimental infection and B38-CAP treatment in hACE2 Tg mice, SARS-CoV-2 strain (UT-NCGM02) was obtained from University of Tokyo and propagated in Vero E6/TMPRSS2 (JCRB Cell Bank, JCRB1819) by infecting at an MOI of 0.01 and then cultured in DMEM containing 2% FBS at 37°C for 3 days, and aliquots of the culture media of the virus were stored at -80°C until use at the Tsukuba Primate Research

Center of NIBIOHN. Virus used for animal experiments was from passages P4. No mutations in the furin cleavage site of Spike were detected in the RNA samples from infected mouse lungs by sequencing (not shown). For treatment with B38-CAP in SARS-CoV-2 infected hamsters, SARS-CoV-2 (JPN/TY/WK-521) was provided from National institute of infectious diseases, Japan, and propagated and passaged in Vero E6/TMPRSS2 cells as previously described [48], and virus of passages P6 was used for experimental infection and B38-CAP treatment in hamsters at Gunma University. All experiments with infectious SARS-CoV-2 were performed in enhanced biosafety level 3 (BSL3) containment laboratories at Tsukuba Primate Research Center of the NIBIOHN, at the University of Tokyo, at the University of Hong Kong or at Gunma University, which followed the approved standard operating procedures of BSL3 facility as previously described [30,31].

Animals

Three and ten week-old male Syrian hamsters were purchased from SLC Japan and maintained at the animal facilities of Akita University or University of Tokyo. Female Syrian hamsters, aged 6 weeks old, were obtained from the Chinese University of Hong Kong Laboratory Animal Service through the Centre Center for Comparative Medicine Research of the University of Hong Kong. Human ACE2 transgenic (hACE2 Tg) mice, which express human ACE2 in the whole body under CAG promoter, were generated and donated by Drs. Akihiko Uda and Kiyoshi Tanabayashi at National Institute of Infectious Diseases. Human ACE2 cDNA was cloned into pCAGGSP7 vector, and founder mice were generated with pronuclear injection of the expression cassette into zygotes and crossed to C57BL/6J mice. All three lines of the mice (#5, #16, #17) were infective of SARS coronavirus (Uda A, Tanabayashi K, et al. manuscript in preparation). The mice had been cryo-archived and were recovered at Laboratory Animal Resource Bank of NIBIOHN (https://animal.nibiohn.go.jp/e_ace2_tg_17.html). The recovered line #17 was efficient in expanding colonies and used in this study, and expression of human ACE2 was confirmed with Western blot, and the genotypes of mice were determined by PCR for tail DNA with the primer pair; 5'-CTTGGTGATATGTGGGGTAGA -3' and 5'- CGCTTCATCTCCCACCACTT -3'. Presence of endogenous mouse Ace2 gene was also confirmed by PCR with the primer pair; 5'- CCGGCTGCTCTTTGAGAGGACA -3'and 5'- CTTCATTGGCTCCGTTTCTTAGC -3'. hACE2 Tg mice were maintained as heterozygous (*hACE2*$^{Tg/+}$) by crossing *hACE2*$^{Tg/+}$mice with wild type mice at the animal facility of NIBIOHN or Akita University. All animal experiments conformed to the Guide for the Care and Use of Laboratory Animals, Eighth Edition, updated by the US National Research Council Committee in 2011, and approvals of the experiments were granted by the ethics review board of Akita University, NIBIOHN, the University of Tokyo or the University of Hong Kong.

Experimental infection of hamsters.

To measure ACE2 protein expression in the infected lungs, experimental infection of hamsters was conducted in enhanced BSL3 laboratory at the University of Tokyo and at the University of Hong Kong. Ten week-old male Syrian hamsters (Japan SLC, Inc.) and 6 week-old female Syrian hamsters (originally from Envigo) were used at the University of Tokyo and at the University of Hong Kong, respectively [30,31].

Under ketamine-xylazine anesthesia, six of 10 week-old male hamsters and five of 6 week-old female hamsters were inoculated via intranasal routes with 10^3 PFU (in 100 µL PBS) of the SARS-CoV-2 (Tokyo strain, UT-NCGM02) and 10^5 PFU (in 100 µL PBS) of the virus (Hong Kong strain, HKU-001a), respectively. At four days after infection, hamsters were euthanized with overdose of anesthesia, lung tissues were harvested for preparation of protein lysates and infectious virus inactivated with heat (92^{o}C, 15 min) and detergent (2% SDS). To investigate the effects of B38-CAP in SARS-CoV-2 infection, 6 week-old male Syrian hamsters (Japan SLC, Inc.) were inoculated via intratracheal routes with 1 x 10^3 $TCID_{50}$ (in 100 µL PBS) of the SARS-CoV-2 (JPN/TY/WK-521, passages P6) under anesthesia with cocktails of 0.2 mg/kg medetomidine, 6 mg/kg midazolam and 10 mg/kg butorphanol tartrate in enhanced BSL3 laboratory at Gunma University. Body weight and survival of infected hamsters were monitored for 4 days, and lung tissues were harvested after euthanasia. Cranial lobes of right lungs were used for measurements of wet to dry weight ratio, and the remaining lobes of right lungs were put in RNAlater for RNA extraction and qRT-PCR or were snap frozen and kept at -80^{o}C until use for peptide extraction for ELISA measurements of Ang II or Ang 1-7. Left lungs were fixed with 4% formalin for histological examination. For B38-CAP treatment, hamsters were infected and divided into two groups. At 12 hours post infection, intraperitoneal injection of B38-CAP (2 mg/kg/day) or vehicle was initiated and repeated once a day. At 4 days after infection, the hamsters were euthanized, left and right lungs were harvested as described above.

Experimental infection of hACE2 Tg mice.

Experimental infection of mice was conducted in enhanced BSL3 laboratory at Tsukuba Primate Research Center of the NIBIOHN. Three to four month-old male hACE2 Tg or littermate wild type mice were inoculated with 2 x 10^3 $TCID_{50}$ of the SARS-CoV-2 (UT-NCGM02, passages P4) in 50 µl PBS via the intratracheal route under anesthesia with cocktails of 0.2 mg/kg medetomidine, 6 mg/kg midazolam and 10 mg/kg butorphanol tartrate. Body weight and survival of infected mice were monitored and mice showing >25% loss of their initial body weight were defined as reaching experimental end-point and humanely killed. For assessment of kinetics of infection and pathologies, independent experiments were performed, infected hACE2 Tg or wild type mice were euthanized and samples were harvested at 2, 4, 6 or 7 dpi. Thirteen organs (lung, nasal turbinate, trachea, brain, heart, liver, pancreas, spleen, kidney, small intestine, colon, anterior tibial muscle, testis) were harvested from each mouse. Excised organs other than lung and brain were snap frozen and homogenized with TRIzol reagent (Invitrogen) using Beads Grinding Machine (BHA-6; AS ONE) in BSL3 laboratory to determine the viral N RNA copy numbers with qRT-PCR. Cranial lobes of right lungs were subjected to measurements of wet to dry weight ratio, and the remaining lobes of right lungs were put in RNAlater for RNA extraction and qRT-PCR or were snap frozen and kept at -80^{o}C until use for homogenization for measurements of $TCID_{50}$, protein extraction for Western blot or peptide extraction for ELISA measurements of Ang II or Ang 1-7. Left lungs were fixed with 4% formalin for histological examination. Right cerebral hemispheres were homogenized for $TCID_{50}$ measurement, and left hemisphere were used for RNA extraction and qRT-PCR. To examine the effects of B38-CAP in SARS-CoV-2 infection, infected mice were divided into two groups, intraperitoneal injection of B38-CAP (2 mg/kg/day) or vehicle was initiated at 12 hours post infection and repeated once a day. At four days

after infection, mice were euthanized, lung samples were harvested as described above. For measurements of lung function, at 4 dpi the mice were anesthetized, tracheostomized, mechanically ventilated and lung function measured with Resistance and Compliance system (Buxco). Pulmonary function parameters of elastance and resistance were obtained under mechanical ventilation with tidal volume (10 ml/kg) and PEEP (2 cm H_2O) for 15 minutes.

Recombinant proteins

The coding sequence of S1 domain (1-685 amino acids) or RBD (319-541 amino acids) of the Spike protein of SARS-CoV-2 were codon optimized, synthesized, and subcloned into the pCAGGS vector to generate a fusion protein with the Fc portion of human IgG1. Human Expi293F cells (Gibco) were transfected with the S1-Fc and RBD-Fc expression vector, supernatants harvested, and S1-Fc and RBD-Fc protein purified by affinity chromatography using a Protein A HP column (Cytiva). Control-Fc protein (#AG714; Merck) was purchased. Trimeric Spike (1-1208 amino acids) with 6 proline substitutions retaining the prefusion conformation (Spike-6P) were prepared as described previously [32]. Recombinant B38-CAP protein was expressed in *E. coli.* and purified as previously described[26]. All the proteins were confirmed free of endotoxin contamination (<0.1 EU/μg protein) with LAL Endotoxin Assay Kit (Genscript).

In vitro binding assays

For pull-down assay to evaluate binding of Spike proteins (S1-Fc and RBD-Fc) to human ACE2 or hamster ACE2 protein, Caco2 human colon epithelial cells or hamster lung tissues were homogenized in lysis buffer (50 mM Tris-HCl, pH 7.4, 1 mM EDTA, 1% NP-40, protease inhibitor (Complete Mini; Roche), 20 mM NaF, and 2 mM Na_3VO_4). Protein lysates were incubated with Spike-6P, S1-Fc, RBD-Fc or control human IgG-Fc protein with gentle agitation for 2 hours at 4℃. S1-Fc, RBD-Fc or control-Fc protein were pulled down by Protein G dynabeads (Thermo Fisher Scientific), while Spike-6P protein were pulled down by HIS-Select® Nickel Affinity Gel (SIGMA). Proteins were separated by SDS-PAGE and transferred to a Nitrocellulose membrane. The membranes were probed with anti-human ACE2 antibody (Novus Biological, SN0754), anti-mouse ACE2 antibody[49] for detection of hamster ACE2 or anti-human IgG antibody (MBL, 103R). For assessment of binding of B38-CAP to RBD-Fc, B38-CAP was detected by B38-CAP-specific polyclonal antibody as previously described [26], and recombinant soluble human ACE2 (R&D systems, 933-ZN) was served as a positive control for binding to RBD-Fc. Flow cytometry analysis to address the effects of RBD-Fc on cell-surface ACE2 expression was done as previously described [10,33]. Briefly, Vero E6 cells are detached by 2 mM EDTA/PBS and incubated with RBD-Fc or control-Fc protein at 4°C or 37°C for 3 hours. Cells were then incubated with FITC-conjugated human IgG-specific polyclonal antibody (Jackson ImmunoResearch, #109-095-088) for detection of RBD-Fc protein and control-Fc bound to Vero E6 cells, and samples were analyzed by flow cytometry using a FACS Calibur (Becton Dickinson).

Spike protein-mediated acute lung injury in hamsters

For acid aspiration-induced acute lung injury, three week-old male hamsters were anesthetized with ketamine (200 mg/kg) and xylazine (10 mg/kg), and were intratracheally instilled with 0.1 M HCl (in 100 µl PBS). For spike plus acid aspiration-induced lung injury, SARS-CoV-2 Spike proteins (Spike-6P (3.7 nmol/kg), S1-Fc (11 nmol/kg) or RBD-Fc (11 nmol/kg)) or control-Fc (11 nmol/kg) were intraperitoneally injected 30 minutes before and at 12 hours after acid aspiration. For B38-CAP treatment, B38-CAP protein (2 mg/kg) or vehicle was *i.p.* injected at 3 and 15 hours after acid instillation. To evaluate lung pathologies, the hamsters were euthanized with overdose of anesthesia at 24 hours after acid instillation, and blood samples were collected with protease-inhibitor cocktails for Ang II and Ang 1-7 measurements with ELISA and lungs were excised *en bloc* with hearts. After taking macro photography of the lungs, the left lobe of lungs, which usually exhibit more severe injury than right lungs, was cut into three pieces to measure wet to dry weight ratio, RNA expression and protein expression, and the posterior lobe of right lungs was fixed with 4% formalin samples for histological analysis. For measurements of lung function, the hamsters were anesthetized with ketamine and xylazine at 17 hours after acid aspiration, tracheostomized, mechanically ventilated and lung function measured with Resistance and Compliance system (Buxco). Pulmonary function parameters; elastance, resistance and dynamic or static compliance were obtained under mechanical ventilation with tidal volume (10 ml/kg) and PEEP (2 cm H_2O) for 15 minutes. After measurements, the hamsters were euthanized with overdose of anesthesia, and heparinized blood samples were collected for measuring ACE2 enzymatic activity.

Histopathology and immunohistochemistry

Lung tissues were fixed with 4% formalin and embedded in paraffin. Five mm thick sections were prepared and stained with Hematoxylin & Eosin (H&E). For semi quantitative assessment of lung injury, the high-resolution images (x200 magnification) of the lung sections stained with H&E were taken with microscope (Nikon). Three randomly chosen fields of each section were scored for Lung injury score in a blinded fashion using a previously defined score consisting of alveolar congestion, hemorrhage, neutrophil infiltration, thickness of alveolar wall, and hyaline membrane formation, as follows: 0 = minimal (little) damage, 1 = mild damage, 2 = moderate damage, 3= severe damage and 4 = maximal damage [50]. The average Lung injury score of three fields of each section were used as the one individual Lung injury score. For immunohistochemistry of S1-Fc or RBD-Fc proteins in the lungs, 5 mm sections were pretreated with EDTA buffer at 72°C and stained with peroxidase-conjugated anti-human Fc antibody (Jackson ImmunoResearch, # 109-035-098).

Western blotting

Lung proteins were extracted with TNE lysis buffer (50 mM Tris, 150 mM NaCl, 1 mM EDTA, 1% NP40, protease inhibitor (Complete Mini; Roche), 20 mM NaF, 2 mM Na_3VO_4) with Microsmash (MS-100R; TOMY), were sonicated and denatured with LDS sample buffer (Invitrogen) at 70°C. For protein extraction from SARS-CoV-2-infected lungs in BSL3 laboratory, 20 mg pieces of the lung tissues were homogenized by using 3-min Total Protein Extraction Kit (P502L; 101Bio), and the lysates were denatured with 1.3x LDS sample buffer (Invitrogen) or 2% SDS at 92°C for 15 minutes. After confirming virus

inactivation, the protein samples were taken out from BSL3 laboratory. Proteins were electrophoresed on NuPAGE bis-tris precast gels (Invitrogen) and transferred to nitrocellulose membranes (Invitrogen). Membranes were probed with following antibodies; anti-mouse ACE2 antibody for detection of mouse or hamster ACE2 [49], anti-hamster GAPDH antibody (GeneTex, GTX100118), anti-SARS-CoV/SARS-CoV-2 NP antibody[30], anti-human ACE2 antibody (R&D systems, MAB9331), anti-b-actin antibody (Sigma, A5316) or anti-human IgG antibody (MBL, 103R). The blotting bands visualized with ECL reagent (Bio-Rad) using ChemiDoc Touch Imaging System (Bio-Rad). Image Lab software was used to quantify band intensity.

Measurements of cytokine mRNA expression by qRT-PCR

qRT-PCR analysis was conducted as previously described [26]. Briefly, total RNA was extracted using TRIzol reagent (Invitrogen) and cDNA synthesized using the PrimeScript RT reagent kit (RR037; TAKARA). Quantitative real-time PCR was run in 96 well plates using a SYBR Premix ExTaq II (RR820; TAKARA) according to the instructions of the manufacturer. Relative gene expression levels were quantified by using the Thermal Cycler Dice Real Time System II software (TAKARA). Sequences of the forward and reverse primers of the genes studied are shown in Extended Data Table 1.

Viral load determination by qRT-PCR

qRT-PCR to quantify viral N gene copies was conducted in 2 steps; reverse transcriptase (RT) reaction and real-time probe qPCR, with modifications of the diagnostic protocol released from National Institute of Infectious Disease in Tokyo, Japan [51]. The primer and probe sequences are: 5'-AAATTTTGGGGACCAGGAAC-3' (forward primer (NIID_2019-nCOV_N_F2)), 5'-TGGCAGCTGTGTAGGTCAAC-3' (reverse primer (NIID_2019-nCOV_N_R2)) and 5'-FAM-ATGTCGCGCATTGGCATGGA-BHQ-3' (probe (NIID_2019-nCOV_N_P2)). cDNA was synthesized using the PrimeScript RT reagent kit (RR037; TAKARA) in 10 ml RT reaction containing 2 ml 5x PrimeScript Buffer, 0.5 ml PrimeScript RT Enzyme Mix, 10 ng/ml total RNA and 1 mM viral N gene-specific primer (NIID_2019-nCOV_N_R2) with the condition of RT at 42°C for 15 min and inactivation of reverse transcriptase at 85°C for 5 s. The RT reaction products were 10-fold diluted, and one ml of the diluents were subjected to quantitative real-time PCR using Probe qPCR kit (RR390A; TAKARA) in 25 ml qPCR reaction containing 12.5 ml 2x Premix Ex Taq and 5 ml 5x NIID_2019-nCOV_N_ Primer/Probe mix (XD0007; TAKARA) with 40 cycles of PCR amplification (Denaturing at 95°C for 5 s; Annealing/Extending at 60°C for 30 s). The expected amplicon size is 158 bp. The standard curve of qRT-PCR was generated by RT reaction with serial 10-fold dilutions of synthesized N RNA fragment (XA0142; TAKARA) with a known copy number (from 1.0×10^6 to 1.0×10^2 copies per µl of RT reaction) in the presence of 10 ng/ml total RNA from uninfected mouse lungs, followed by the real-time probe qPCR with one µl of the 10-fold-diluted RT reaction products. These dilutions were used as quantification standards to construct the standard curve by plotting the RNA copy number against the corresponding threshold cycle values (Ct). Results were expressed as log10-transformed numbers of viral N RNA copy numbers per gram of the lung tissues.

Measurements of Ang II and Ang 1-7 levels and ACE2 activity

Plasma Ang II levels were measured with ELISA assay after peptide extraction as previously described [26]. Briefly, blood samples were collected in tubes containing EDTA (25 mM), o-phenanthroline (0.44 mM), pepstatin A (0.12 mM), and p-hydroxymercuribenzoic acid (1 mM), and then centrifuged at 1,200 x g for 10 min. Angiotensin peptides were acidified and extracted with Sep-Pak cartridges (Waters), and Ang II in the peptide extract was quantified using an ELISA kit (Enzo Life Sciences). Plasma Ang 1–7 concentrations were also determined by subjecting the peptide extracts to measurements with Ang 1–7 ELISA kit (CUSABIO Biotech). To measure the Ang II or Ang 1-7 levels in the lung lysates, frozen lung tissues were homogenized in ice-cold 0.5% formic acid containing 0.5 mg/ml aprotinin and 12.5 mM EDTA, and angiotensin peptides were extracted with Sep-Pak cartridges and the eluates were subjected to ELISA measurements. The measurements for infectious samples were performed in enhanced BSL3 laboratory. Plasma ACE2 activity was measured as previously described [26]. Heparinized plasma was diluted with assay buffer, and the reaction mixture contained 40 µl of HEPES buffer, pH 7.5, 0.3 M NaCl, 20 µM Nma-Leu-Pro-Lys(Dnp), 0.01% Triton X-100, 0.02% NaN_3, 5 µl diluted plasma and 5 ml of the HEPES buffer with or without 10µg/ml MLN-4760, an ACE2 inhibitor in a total volume of 50 µl. The reaction mixture was incubated at 37 ^oC for 60 min and then the reaction was terminated by adding 0.2 ml of 0.1 M sodium borate buffer pH 10.5, and the fluorescence intensity was measured. Plasma ACE2 activity was determined by subtracting the fluorescence intensity with MLN-4760 from the one without MLN-4760.

Measurement of SARS-CoV-2 replication by $TCID_{50}$

To measure the viral titer in the lung and brain, the tissues were homogenized in 10 times volumes of the tissue weight of lysis buffer (20 mM Hepes-NaOH (pH7.4), 150 mM NaCl) using Beads Grinding Machine (BHA-6; AS ONE) in BSL3 laboratory. Tissue lysates were serially diluted by a factor of 10 with RPMI1640 containing 5% FBS and penicillin-streptomycin. The diluted lysates were incubated with Vero E6/TMRPSS2 cells (2 x 10^4 cells/well) in 96 well plates for 3 days, and viral titers of each sample were calculated using the Reed-Muench calculation method.

Neutralization of cell entry and replication of SARS-CoV-2 by using B38-CAP in vitro

To assess the effects of B38-CAP on cell entry of SARS-CoV-2, both B38-CAP (0, 25, 50 or 100 µg/ml) and SARS-CoV-2 (MOI 0.05) were added to the culture of Vero E6/TMPRSS2 cells (3 x 10^4 cells/well) in 12 well plates for 1 hour, and then the cells were washed three times with PBS and incubated with fresh growth medium of RPMI1640 containing 5% FBS and penicillin-streptomycin. For effects of B38-CAP treatment on progeny virus, Vero E6/TMPRSS2 cells were infected with SARS-CoV-2 (MOI 0.05) for 1 hour, washed three times with PBS and incubated with fresh medium containing B38-CAP (0, 25, 50 or 100 µg/ml). Cell lysates were harvested with TRIzol reagent (Invitrogen) at 20 hours post infection, and viral N RNA abundance was measured with qRT-PCR.

Measurements of markers for tissue injury and liver and kidney functions

Plasma levels of Lactate dehydrogenase (LDH), Aspartate transaminase (AST) or Alanine transaminase (ALT), Creatinine (Cr) and Blood Urea Nitrogen (BUN) were measured as markers of liver and kidney damages, respectively, by using FUJI DRI-CHEM slide kits (Fujifilm corporation).

Statistical analyses. Data are presented as mean values ± SEM. Statistical significance between two experimental groups was determined using Student's two-tailed *t*-test. Comparisons of parameters among more than 3 groups were analyzed by one-way ANOVA, followed by Sidak's multiple comparisons test. When a comparison is done for groups with two factor levels, two-way ANOVA with Sidak's multiple comparisons test were used. $P < 0.05$ was considered significant.

Declarations

Data Availability

The data that support the findings of this study are available from the corresponding author upon reasonable request. Source data used to generate Figs. 1-4 and Extended Data Figs. 1-7 are provided in the Source Data file.

Funding

K.K. is supported by the Kaken [20H03426, 20K21566] from Japanese Ministry of Science, the FY2020 Program to Develop Countermeasure Technologies against Viral and Other Infectious Diseases [24-136] from Japan Agency for Medical research and Development (AMED) and the Naito Foundation. Y.I. is supported by the Kaken [17H06179], T.Y. is supported by the Kaken [20K07285] from Japanese Ministry of Science and Takeda Science Foundation, J.A. is supported by the Kaken [20K16153] from Japanese Ministry of Science, and J.F.-W.C. is supported by Lo Ying Shek Chi Wai Foundation and the National Program on Key Research Project of China [2020YFA0707500 and 2020YFA0707504]. J.M.P. received funding from the T. von Zastrow foundation, the FWF Wittgenstein award (Z 271-B19), the Austrian Academy of Sciences, the Innovative Medicines Initiative 2 Joint Undertaking (JU) under grant agreement No 101005026, and the Canada 150 Research Chairs Program F18-01336 as well as the Canadian Institutes of Health Research COVID-19 grants F20-02343 and F20-02015.

Acknowledgments

We thank all members of our laboratories for technical assistance and helpful discussions. We thank Dr. Kiyoshi Tanabayashi at National Institute of Infectious Diseases for providing hACE2 Tg mice.

Author Contributions

T.Y., M.H., T.M., Y.I. and K.K. conceived the study. T.Y., M.H., T.M., J.A., A.S., S.T., Y.F., S.M., J.M.P., Y.I. and K.K. conducted experiments and/or analyzed data. S.Nirasawa, M.N., S.Nagata. and H.K. prepared recombinant proteins. T.Y., M.N.A., M.I., A.U., J.F.-W.C., R.N., D.U., V.K.P., A.Y., C.C.-S.Y., K.-Y.Y., W.K., K.M., Y.K., Y.Y. and K.K conducted infection experiments. K.K. wrote the manuscript with input from all authors.

Competing Interests

J.M.P. is shareholder of Apeiron Biologics which is developing soluble ACE2 (APN01) for COVID-19 therapy.

References

1 Drosten, C. *et al.* Identification of a novel coronavirus in patients with severe acute respiratory syndrome. *N Engl J Med* **348**, 1967-1976, doi:10.1056/NEJMoa030747 (2003).

2 Lee, N. *et al.* A major outbreak of severe acute respiratory syndrome in Hong Kong. *N Engl J Med* **348**, 1986-1994, doi:10.1056/NEJMoa030685 (2003).

3 Peiris, J. S. *et al.* Coronavirus as a possible cause of severe acute respiratory syndrome. *Lancet* **361**, 1319-1325, doi:10.1016/s0140-6736(03)13077-2 (2003).

4 Zhou, P. *et al.* A pneumonia outbreak associated with a new coronavirus of probable bat origin. *Nature* **579**, 270-273, doi:10.1038/s41586-020-2012-7 (2020).

5 Zhu, N. *et al.* A Novel Coronavirus from Patients with Pneumonia in China, 2019. *N Engl J Med* **382**, 727-733, doi:10.1056/NEJMoa2001017 (2020).

6 Zhou, F. *et al.* Clinical course and risk factors for mortality of adult inpatients with COVID-19 in Wuhan, China: a retrospective cohort study. *Lancet* **395**, 1054-1062, doi:10.1016/S0140-6736(20)30566-3 (2020).

7 Guan, W. J. *et al.* Clinical Characteristics of Coronavirus Disease 2019 in China. *N Engl J Med* **382**, 1708-1720, doi:10.1056/NEJMoa2002032 (2020).

8 Chan, J. F. *et al.* A familial cluster of pneumonia associated with the 2019 novel coronavirus indicating person-to-person transmission: a study of a family cluster. *Lancet* **395**, 514-523, doi:10.1016/S0140-6736(20)30154-9 (2020).

9 Li, W. *et al.* Angiotensin-converting enzyme 2 is a functional receptor for the SARS coronavirus. *Nature* **426**, 450-454, doi:10.1038/nature02145 (2003).

10 Kuba, K. *et al.* A crucial role of angiotensin converting enzyme 2 (ACE2) in SARS coronavirus-induced lung injury. *Nat Med* **11**, 875-879, doi:10.1038/nm1267 (2005).

11 Shang, J. *et al.* Structural basis of receptor recognition by SARS-CoV-2. *Nature* **581**, 221-224, doi:10.1038/s41586-020-2179-y (2020).

12 Wrapp, D. *et al.* Cryo-EM structure of the 2019-nCoV spike in the prefusion conformation. *Science* **367**, 1260-1263, doi:10.1126/science.abb2507 (2020).

13 Donoghue, M. *et al.* A novel angiotensin-converting enzyme-related carboxypeptidase (ACE2) converts angiotensin I to angiotensin 1-9. *Circ Res* **87**, E1-9, doi:10.1161/01.res.87.5.e1 (2000).

14 Tipnis, S. R. *et al.* A human homolog of angiotensin-converting enzyme. Cloning and functional expression as a captopril-insensitive carboxypeptidase. *J Biol Chem* **275**, 33238-33243, doi:10.1074/jbc.M002615200 (2000).

15 Corvol, P., Jeunemaitre, X., Charru, A., Kotelevtsev, Y. & Soubrier, F. Role of the renin-angiotensin system in blood pressure regulation and in human hypertension: new insights from molecular genetics. *Recent Prog Horm Res* **50**, 287-308, doi:10.1016/b978-0-12-571150-0.50017-2 (1995).

16 Skeggs, L. T., Dorer, F. E., Levine, M., Lentz, K. E. & Kahn, J. R. The biochemistry of the renin-angiotensin system. *Adv Exp Med Biol* **130**, 1-27 (1980).

17 Gheblawi, M. *et al.* Angiotensin-Converting Enzyme 2: SARS-CoV-2 Receptor and Regulator of the Renin-Angiotensin System: Celebrating the 20th Anniversary of the Discovery of ACE2. *Circ Res* **126**, 1456-1474, doi:10.1161/CIRCRESAHA.120.317015 (2020).

18 Imai, Y. *et al.* Angiotensin-converting enzyme 2 protects from severe acute lung failure. *Nature* **436**, 112-116, doi:10.1038/nature03712 (2005).

19 Yang, P. *et al.* Angiotensin-converting enzyme 2 (ACE2) mediates influenza H7N9 virus-induced acute lung injury. *Sci Rep* **4**, 7027, doi:10.1038/srep07027 (2014).

20 Zou, Z. *et al.* Angiotensin-converting enzyme 2 protects from lethal avian influenza A H5N1 infections. *Nat Commun* **5**, 3594, doi:10.1038/ncomms4594 (2014).

21 Ziegler, C. G. K. *et al.* SARS-CoV-2 Receptor ACE2 Is an Interferon-Stimulated Gene in Human Airway Epithelial Cells and Is Detected in Specific Cell Subsets across Tissues. *Cell* **181**, 1016-1035 e1019, doi:10.1016/j.cell.2020.04.035 (2020).

22 Onabajo, O. O. *et al.* Interferons and viruses induce a novel truncated ACE2 isoform and not the full-length SARS-CoV-2 receptor. *Nat Genet* **52**, 1283-1293, doi:10.1038/s41588-020-00731-9 (2020).

23 Oudit, G. Y. *et al.* Human recombinant ACE2 reduces the progression of diabetic nephropathy. *Diabetes* **59**, 529-538, doi:10.2337/db09-1218 (2010).

24 Zhong, J. *et al.* Angiotensin-converting enzyme 2 suppresses pathological hypertrophy, myocardial fibrosis, and cardiac dysfunction. *Circulation* **122**, 717-728, 718 p following 728, doi:10.1161/CIRCULATIONAHA.110.955369 (2010).

25 Monteil, V. *et al.* Inhibition of SARS-CoV-2 Infections in Engineered Human Tissues Using Clinical-Grade Soluble Human ACE2. *Cell* **181**, 905-913 e907, doi:10.1016/j.cell.2020.04.004 (2020).

26 Minato, T. *et al.* B38-CAP is a bacteria-derived ACE2-like enzyme that suppresses hypertension and cardiac dysfunction. *Nat Commun* **11**, 1058, doi:10.1038/s41467-020-14867-z (2020).

27 Vickers, C. *et al.* Hydrolysis of biological peptides by human angiotensin-converting enzyme-related carboxypeptidase. *J Biol Chem* **277**, 14838-14843, doi:10.1074/jbc.M200581200 (2002).

28 Duarte, M. *et al.* Telmisartan for treatment of Covid-19 patients: An open multicenter randomized clinical trial. *EClinicalMedicine* **37**, 100962, doi:10.1016/j.eclinm.2021.100962 (2021).

29 Semenzato, L. *et al.* Antihypertensive Drugs and COVID-19 Risk: A Cohort Study of 2 Million Hypertensive Patients. *Hypertension* **77**, 833-842, doi:10.1161/HYPERTENSIONAHA.120.16314 (2021).

30 Chan, J. F. *et al.* Simulation of the clinical and pathological manifestations of Coronavirus Disease 2019 (COVID-19) in golden Syrian hamster model: implications for disease pathogenesis and transmissibility. *Clin Infect Dis*, doi:10.1093/cid/ciaa325 (2020).

31 Imai, M. *et al.* Syrian hamsters as a small animal model for SARS-CoV-2 infection and countermeasure development. *Proc Natl Acad Sci U S A* **117**, 16587-16595, doi:10.1073/pnas.2009799117 (2020).

32 Hsieh, C. L. *et al.* Structure-based design of prefusion-stabilized SARS-CoV-2 spikes. *Science* **369**, 1501-1505, doi:10.1126/science.abd0826 (2020).

33 Wang, S. *et al.* Endocytosis of the receptor-binding domain of SARS-CoV spike protein together with virus receptor ACE2. *Virus Res* **136**, 8-15, doi:10.1016/j.virusres.2008.03.004 (2008).

34 Haga, S. *et al.* Modulation of TNF-alpha-converting enzyme by the spike protein of SARS-CoV and ACE2 induces TNF-alpha production and facilitates viral entry. *Proc Natl Acad Sci U S A* **105**, 7809-7814, doi:10.1073/pnas.0711241105 (2008).

35 Lambert, D. W. *et al.* Tumor necrosis factor-alpha convertase (ADAM17) mediates regulated ectodomain shedding of the severe-acute respiratory syndrome-coronavirus (SARS-CoV) receptor, angiotensin-converting enzyme-2 (ACE2). *J Biol Chem* **280**, 30113-30119, doi:10.1074/jbc.M505111200 (2005).

36 Bao, L. *et al.* The pathogenicity of SARS-CoV-2 in hACE2 transgenic mice. *Nature* **583**, 830-833, doi:10.1038/s41586-020-2312-y (2020).

37 Boudewijns, R. *et al.* STAT2 signaling restricts viral dissemination but drives severe pneumonia in SARS-CoV-2 infected hamsters. *Nat Commun* **11**, 5838, doi:10.1038/s41467-020-19684-y (2020).

38 Song, E. *et al.* Neuroinvasion of SARS-CoV-2 in human and mouse brain. *J Exp Med* **218**, doi:10.1084/jem.20202135 (2021).

39 Lei, Y. *et al.* SARS-CoV-2 Spike Protein Impairs Endothelial Function via Downregulation of ACE 2. *Circ Res* **128**, 1323-1326, doi:10.1161/CIRCRESAHA.121.318902 (2021).

40 Hagiwara, S., Iwasaka, H., Matumoto, S., Hidaka, S. & Noguchi, T. Effects of an angiotensin-converting enzyme inhibitor on the inflammatory response in in vivo and in vitro models. *Crit Care Med* **37**, 626-633, doi:10.1097/CCM.0b013e3181958d91 (2009).

41 Liu, Q. *et al.* miRNA-200c-3p is crucial in acute respiratory distress syndrome. *Cell Discov* **3**, 17021, doi:10.1038/celldisc.2017.21 (2017).

42 Mancia, G., Rea, F., Ludergnani, M., Apolone, G. & Corrao, G. Renin-Angiotensin-Aldosterone System Blockers and the Risk of Covid-19. *N Engl J Med* **382**, 2431-2440, doi:10.1056/NEJMoa2006923 (2020).

43 Reynolds, H. R. *et al.* Renin-Angiotensin-Aldosterone System Inhibitors and Risk of Covid-19. *N Engl J Med* **382**, 2441-2448, doi:10.1056/NEJMoa2008975 (2020).

44 de Abajo, F. J. *et al.* Use of renin-angiotensin-aldosterone system inhibitors and risk of COVID-19 requiring admission to hospital: a case-population study. *Lancet* **395**, 1705-1714, doi:10.1016/S0140-6736(20)31030-8 (2020).

45 Klein, N. *et al.* Angiotensin-(1-7) protects from experimental acute lung injury. *Crit Care Med* **41**, e334-343, doi:10.1097/CCM.0b013e31828a6688 (2013).

46 Nasseri, S. *et al.* Kinin B1 Receptor Antagonist BI113823 Reduces Acute Lung Injury. *Crit Care Med* **43**, e499-507, doi:10.1097/CCM.0000000000001268 (2015).

47 Sodhi, C. P. *et al.* Attenuation of pulmonary ACE2 activity impairs inactivation of des-Arg(9) bradykinin/BKB1R axis and facilitates LPS-induced neutrophil infiltration. *Am J Physiol Lung Cell Mol Physiol* **314**, L17-L31, doi:10.1152/ajplung.00498.2016 (2018).

48 Matsuyama, S. *et al.* Enhanced isolation of SARS-CoV-2 by TMPRSS2-expressing cells. *Proc Natl Acad Sci U S A* **117**, 7001-7003, doi:10.1073/pnas.2002589117 (2020).

49 Crackower, M. A. *et al.* Angiotensin-converting enzyme 2 is an essential regulator of heart function. *Nature* **417**, 822-828, doi:10.1038/nature00786 (2002).

50 Imai, Y. *et al.* Comparison of lung protection strategies using conventional and high-frequency oscillatory ventilation. *J Appl Physiol (1985)* **91**, 1836-1844, doi:10.1152/jappl.2001.91.4.1836 (2001).

51 Shirato, K. *et al.* Development of Genetic Diagnostic Methods for Detection for Novel Coronavirus 2019(nCoV-2019) in Japan. *Jpn J Infect Dis***73**, 304-307, doi:10.7883/yoken.JJID.2020.061 (2020).

Figures

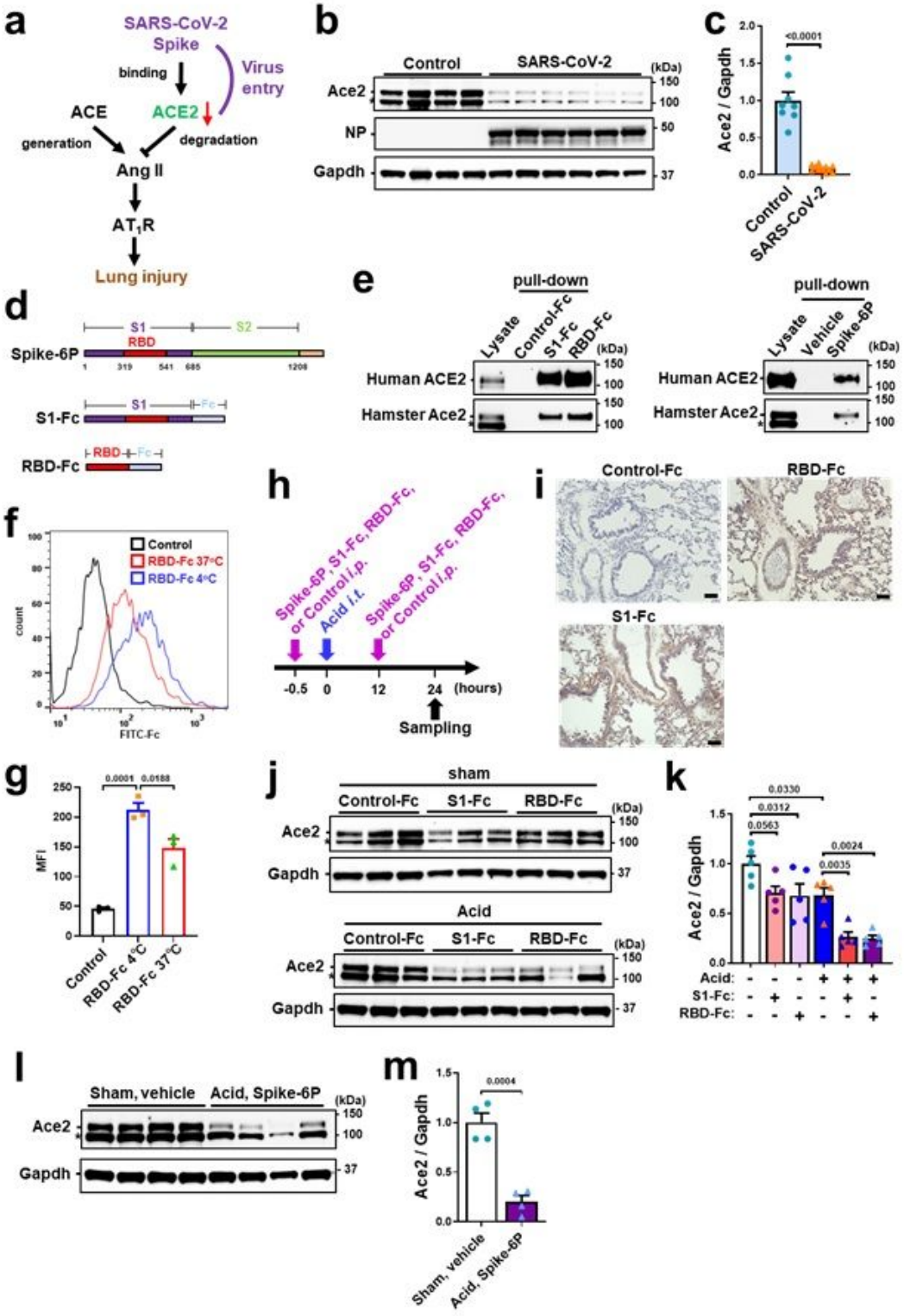

Figure 1

Downregulation of ACE2 expression in lung by SARS-CoV-2. a, Schematic drawing of renin-angiotensin system (RAS) and ACE2 in lung injury. Downregulation of ACE2 expression in SARS-CoV-2 infection is implicated by the studies on SARS coronavirus. b-c, Protein expression of ACE2 in hamster lungs at 4 days after intranasal infection of SARS-CoV-2. Western blot of lung lysates from the hamsters infected with SARS-CoV-2 (UT-NCGM02) (b) are shown. NP; Nucleocapsid phosphoprotein. *; unfolded or short

form of ACE2 or non-specific band. Infection with the HKU-001a strain is shown in Extended Data Fig. 1b. Quantification of ACE2 protein abundance (c) was done with combined results of the two virus strains; uninfected control (n = 8) and SARS-CoV-2 infection (n = 11). Values are means ± SEM. Two-tailed unpaired t-test. d, Constructs of recombinant Spike proteins; Spike-6P, S1-Fc and RBD-Fc. e, Binding of S1-Fc, RBD-Fc or Spike-6P to human ACE2 and hamster ACE2 in pull-down assays. S1-Fc, RBD-Fc and Spike-6P but not control-Fc or vehicle pulled down human ACE2 and hamster ACE2 from lysates of Caco2 human colon cells and hamster lungs, respectively. Total lysates are shown as controls. *; unfolded or short form of ACE2 or non-specific band. Western Blot of S1-Fc, RBD-Fc or Spike-6P are shown in Extended Data Fig. 1d-g. f-g, Decreased cell-surface expression of ACE2 after binding to Spike RBD-Fc protein at 37 °C compared to 4 °C in Vero E6 cells. ACE2 surface expression was detected at 3 h of incubation with RBD-Fc using Fc-specific antibody to directly detect surface-bound RBD-Fc and to avoid masking of the ACE2 epitope. Representative FACS histograms (f) and quantification of mean fluorescence intensity (g) are shown including a background control with an isotype-matched antibody (n = 3 per group). FSC/SSC plot was gated for live and healthy Vero E6 cells. One-way ANOVA with Sidak's multiple comparisons test. Numbers above square brackets show P values. h, Experimental protocol of acid and Spike protein (Spike-6P, S1-Fc or RBD-Fc)-induced lung injury in hamsters. S1-Fc, RBD-Fc, control-Fc (11 nmol/kg for each) or Spike-6P (3.7 nmol/kg) was intraperitoneally injected, and acid was intratracheally instilled (0.1N HCl, 100 ml per body i.t.) under anesthesia. i, Immunohistochemistry of hamster lungs to detect S1-Fc, RBD-Fc or control-Fc protein using a human Fc–specific antibody. Injected S1-Fc or RBD-Fc but not control-Fc localizes to bronchial epithelial cells, inflammatory cells and alveolar pneumocytes. Bars indicate 100 mm. j-m, ACE2 protein expression in hamster lungs. Representative Western blot (j, l) and quantification of ACE2 protein abundance (k, m) are shown (n = 4-5 hamsters per group). *; unfolded or short form of ACE2 or non-specific band. All values are means ± SEM. Two-way ANOVA with Sidak's multiple comparisons test (k) or two-tailed unpaired t-test (m). Numbers above square brackets show significant or nearly significant P values. Independent experiments were performed one time (b, e-g) or two times (c, i-m), and consistent results were obtained.

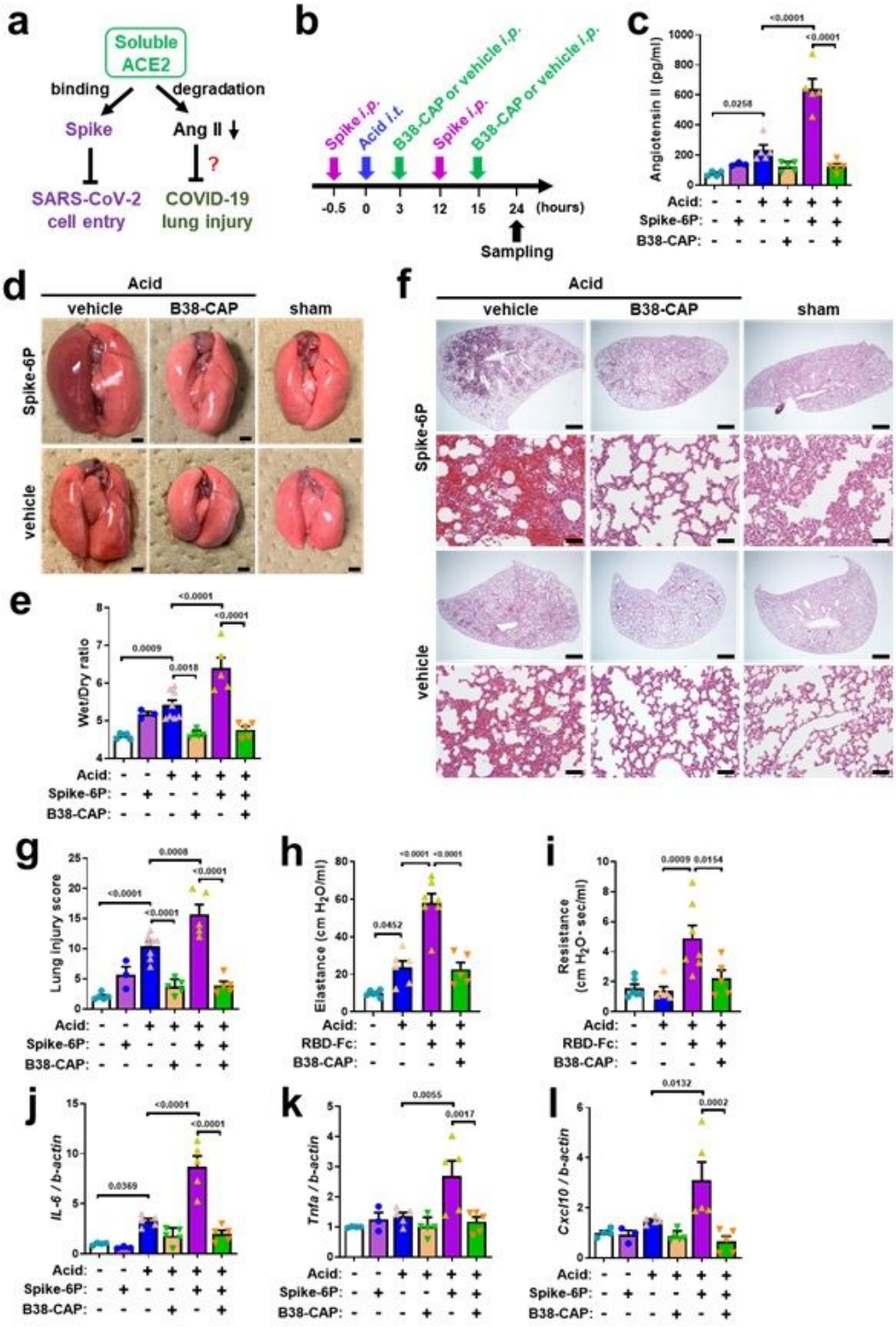

Figure 2

Suppression of SARS-CoV-2 Spike-induced lung injury by B38-CAP. a, Effects of soluble ACE2 in SARS-CoV-2 infection and lung injury. b, Experimental protocol of B38-CAP treatment for hamsters with acid and Spike-induced lung injury. Spike (trimeric Spike-6P protein (3.7 nmol/kg) or RBD-Fc (11 nmol/kg)) or control with or without B38-CAP (2 mg/kg) were intraperitoneally injected (i.p.), and acid (0.1N HCl, 100 ml per body) was intratracheally instilled (i.t.) under anesthesia. c, Plasma Ang II measurements at 24

hours after acid instillation (n = 6-8 hamsters per group). d, Representative photograph of hamster lungs. Bars indicate 2 mm. e, Wet to dry weight ratios of lungs at 24 hours after acid instillation (n = 6-8 hamsters per group). f-g, Lung histopathology. Tissue samples were harvested at 24 hours after acid instillation. Representative images are shown (f). Bars indicate 1 mm (upper) and 100 mm (bottom) for each treatment. Lung injury score measurements (g) (n = 6-8 hamsters per group). h-i, Lung function measurements. Elastance (h) and resistance (i) were measured at 17 hours after acid instillation (n = 5-7 hamsters per group). j-l, qRT-PCR analysis of pro-inflammatory cytokine expression in the lungs of hamsters; mRNA levels of IL-6 (j), TNF-a (k) and CXCL10 (l) normalized with b-actin (n = 5-8 hamsters per group). All values are means ± SEM. One-way ANOVA with Sidak's multiple comparisons test. Numbers above square brackets show significant P values. Independent experiments were performed two times (c-l), and consistent results were obtained.

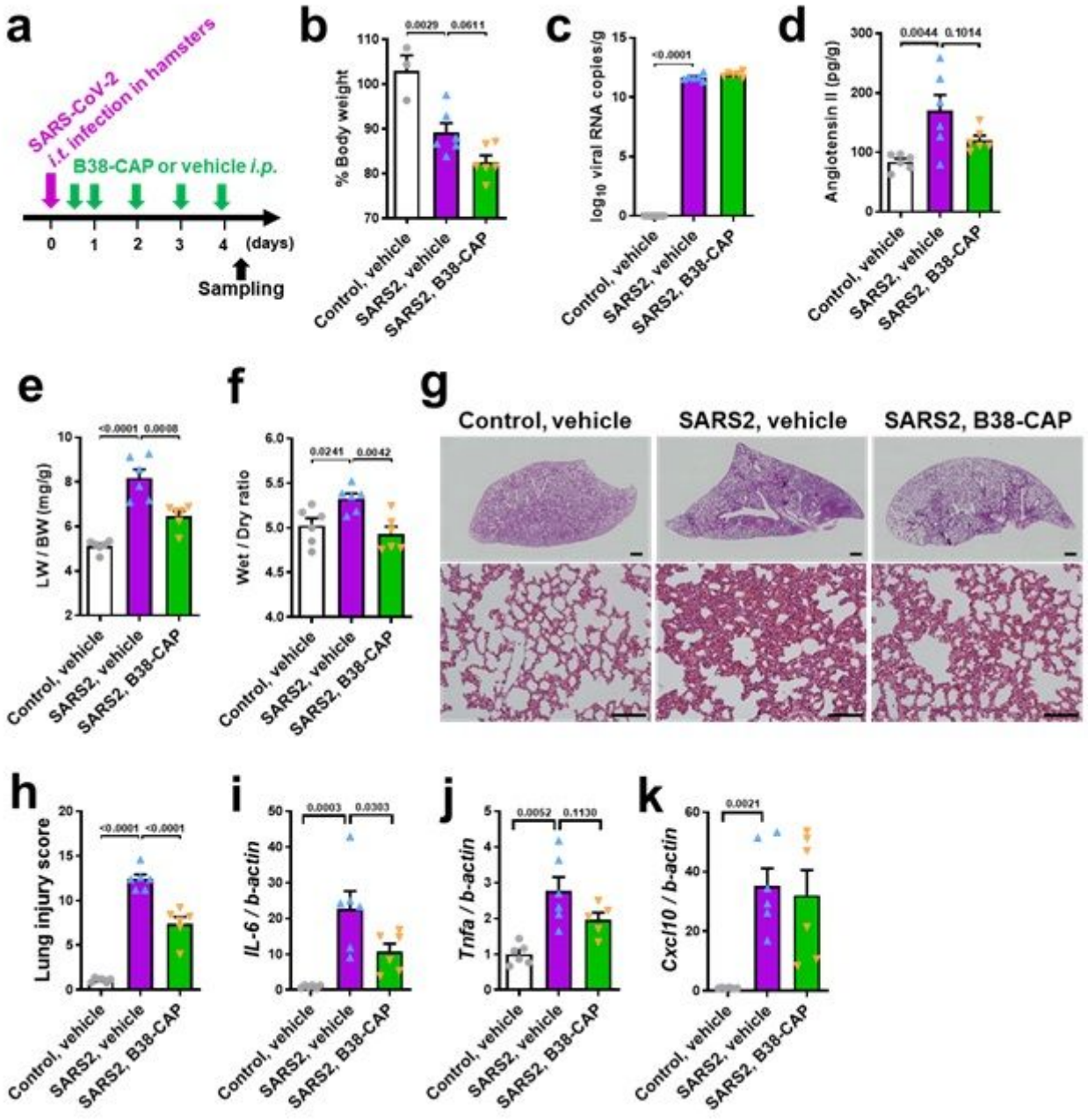

Figure 3

B38-CAP suppresses SARS-CoV-2-induced lung injury in hamsters. a, Experimental protocol; Hamsters were intratracheally infected (i.t.) with SARS-CoV-2 (1 x 103 TCID50), and then the hamsters were injected with B38-CAP (2 mg/kg i.p.) or vehicle once a day. Uninfected control hamsters treated with vehicle (n = 3 (b) or n = 6 (c-k)), SARS-CoV-2 infected hamsters (SARS2) treated with vehicle (n = 6) and SARS2 treated with B38-CAP (n = 6). b, %Changes of body weight at 4 days after infection from before infection. c, qRT-PCR of virus N gene expression in the lungs of hamsters. d, Angiotensin II levels in the lung tissues. e-f, Lung edema measurements. Lung weight to body weight ratio (e) and wet to dry ratio of lung weight (f) are shown. g-h, Lung histopathology. Representative images are shown (g). Bars indicate 1 mm (upper) and 100 mm (bottom). Lung injury scores were measured (h). i-k, qRT-PCR analysis of pro-inflammatory cytokine expression in the lungs of hamsters; mRNA levels of IL-6 (i), TNF-a (j) and CXCL10 (k) normalized with b-actin. All values are means ± SEM. One-way ANOVA with Sidak's multiple comparisons test. Numbers above square brackets show P values. Independent experiments were performed two times (b-k), and consistent results were obtained.

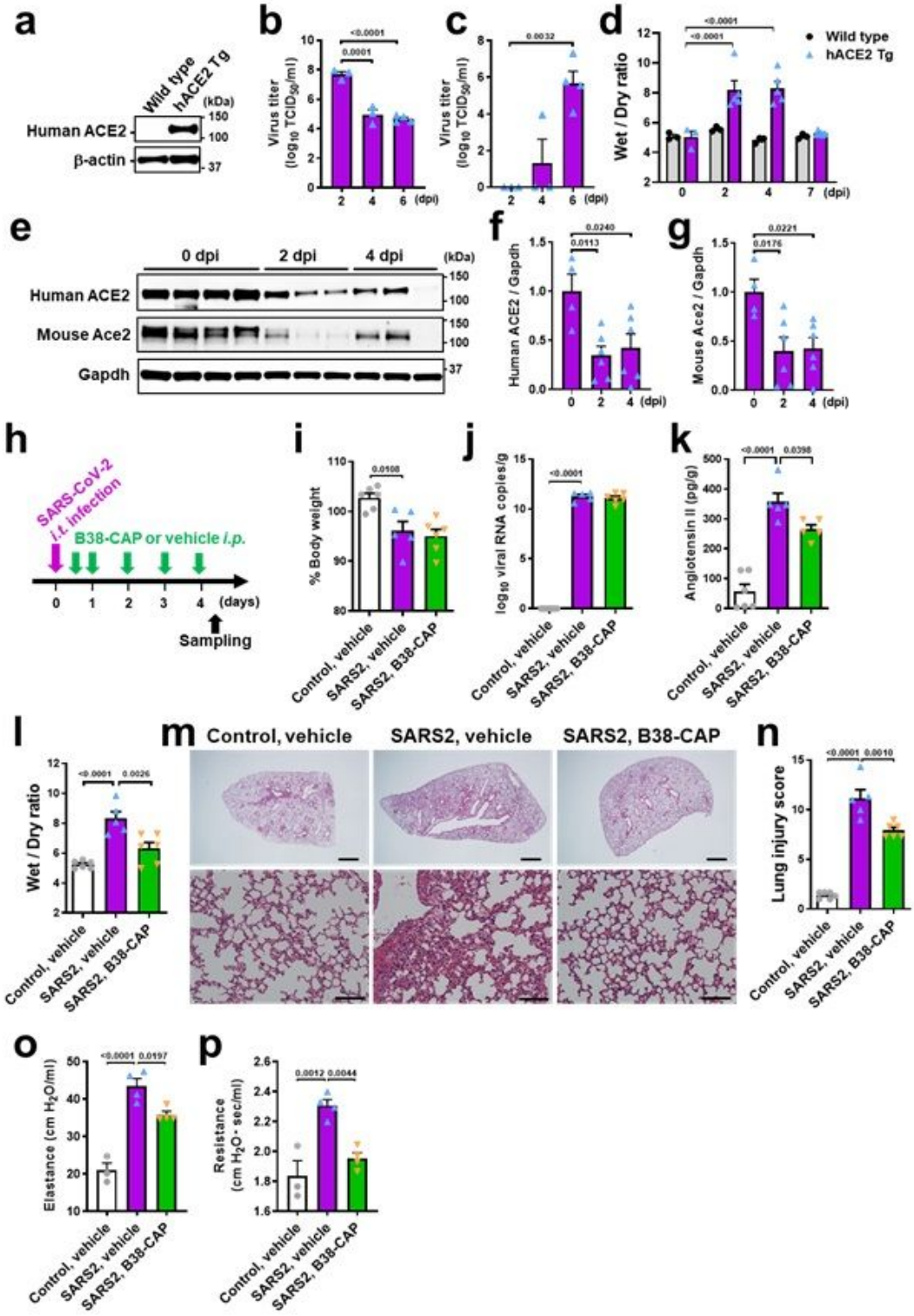

Figure 4

B38-CAP improves SARS-CoV-2-induced lung injury and respiratory dysfunction in hACE2 Tg mice. a, Western blot of human ACE2 protein in the lung lysates from uninfected mice; hACE2 Tg mouse expressing human ACE2 under CAG promoter and its littermate wild type mouse. b-c, Virus titers in hACE2 Tg mice. TCID50 were measured for the lysates of lung (b) and brain (c) prepared from hACE2 Tg mice intratracheally (i.t.) infected with SARS-CoV-2 (2 x 103 TCID50). dpi; days post infection. d, Lung edema

of wild type and hACE2 Tg mice after SARS-CoV-2 infection. Wet to dry ratio of lung weight were measured (n = 3-5). e-g, Protein expression of human ACE2 and mouse Ace2 in the lungs of SARS-CoV-2-infected hACE2 Tg mice. Representative Western blots are shown (e). Human ACE2 (f) and mouse Ace2 (g) were normalized with Gapdh (n = 4-6). h, Experimental protocol; hACE2 Tg mice were i.t. infected with SARS-CoV-2 (2 x 103 TCID50), and then the mice were injected with B38-CAP (2 mg/kg i.p.) or vehicle once a day. Uninfected hACE2 Tg mice (control) treated with vehicle (n = 6), SARS-CoV-2 infected hACE2 Tg mice (SARS2) treated with vehicle (n = 5) and SARS2 treated with B38-CAP (n = 6). i, %Changes of body weight at 4 days after infection from before infection. j, qRT-PCR of virus N gene expression in the lungs of hACE2 Tg mice. k, Angiotensin II levels in the lung tissues. l, Wet to dry ratio of lung weight. m-n, Lung histopathology. Representative images are shown (m). Bars indicate 1 mm (upper) and 100 mm (bottom). Lung injury scores were measured (n). o-p, Lung function measurements. Elastance (o) and resistance (p) were measured at 4 days after SARS-CoV-2 infection in hACE2 Tg mice; control with vehicle treatment (n = 3), SARS2 with vehicle (n = 4) and SARS2 with B38-CAP (n =4). All values are means ± SEM. One-way ANOVA with Sidak's multiple comparisons test. Numbers above square brackets show P values. Independent experiments were performed one time (b, c), two times (a, d-g, o-p) or three times (i-n), and consistent results were obtained.

Supplementary Files

This is a list of supplementary files associated with this preprint. Click to download.

- 210713SARS2ExtendedDataTable15.pdf
- 210715SARS2ExtendedDataFig.17.pdf